Gondwana Research 18 (2010) 632–637

Contents lists available at ScienceDirect

Gondwana Research

journal homepage: www.elsevier.com/locate/gr

Reconstruction of paleo-redox conditions and early sulfur cycling during deposition of the Cryogenian Datangpo Formation in South China

Lian-Jun Feng [a,*], Xue-Lei Chu [a,b], Jing Huang [a,b], Qi-Rui Zhang [a], Hua-Jin Chang [a,b]

[a] Institute of Geology and Geophysics, Chinese Academy of Sciences, Beijing 100029, China
[b] Key Laboratory for Mineral Resources, Chinese Academy of Sciences, Beijing 100029, China

ARTICLE INFO

Article history:
Received 25 July 2009
Received in revised form 25 January 2010
Accepted 8 February 2010
Available online 25 February 2010

Keywords:
Redox conditions
Cryogenian
Iron species
Molybdenum
Sulfur isotope

ABSTRACT

In South China, the Datangpo black shales (663 Ma–654.5 Ma) were deposited during the Cryognian interglacial time between the Sturtian and Marinoan glaciations. Multi-geochemical proxies, including different iron speciation and relevant ratios (Fe_{HR}/Fe_T, Fe_P/Fe_{HR} and Fe_T/Al ratios) and molybdenum concentrations, were used to reconstruct the paleo-depositional environment of this black shale horizon. The ratios of different iron species ($Fe_{HR}/Fe_T>0.38$ and $Fe_P/Fe_{HR}<0.80$) suggest an overall anoxic conditions (ferruginous) over the deposition of the black shales, although intermittent euxinic ($Fe_{HR}/Fe_T>0.38$ and $Fe_P/Fe_{HR}\approx0.80$) and oxic ($Fe_{HR}/Fe_T<0.38$) intervals could have occurred. Furthermore, Fe_T/Al ratios ($Fe_T/Al\leq0.51$) confirm that water column may not be persistent euxinia during the deposition of the Datangpo black shales. Meanwhile, molybdenum concentrations show a decreasing trend towards the top of the black shales, reconciling the gradual oxygenating trend during this period as stated above. Compared to $\delta^{34}S_{Py}$ values in the Mesoproterozoic deep ocean, more positive $\delta^{34}S_{Py}$ values of this study may result from a small size of sulfate reservoir. The small-size sulfate reservoir and concurrent enrichment of molybdenum indicate that the ocean chemistry in the Cryogenian Period is similar to that in the Archean Eon.

1. Introduction

The Neoproterozoic Era (1000–542 Ma) was an important interval subjected to dramatic climatic changes and biological evolutions in Earth's history. The Snowball Earth hypothesis suggested that the Earth was completely covered by ice sheets during the Neoproterozoic glaciation epoches (Hoffman et al., 1998). In the aftermath of glaciations, several lines of evidence, including iron chemistry and sulfur isotopic data from China, Canada, Oman and Australia, indicate stepwise oxygenation of the postglacial Ediacaran ocean (635–542 Ma), stimulating the evolution of early animal life (Canfield et al., 2007; Fike et al., 2006; Komiya et al., 2008; Maruyama and Santosh, 2008; McFadden et al., 2008). South China block provides a unique window to shed light on the early animal evolution where many biota, i.e., the Doushantuo and Weng'an biota, appeared during the Ediacaran Period (635–542 Ma) (Chen et al., 2000; Li et al., 2008; Ohno et al., 2008; Xiao et al., 1998). Until now, variable geochemical signatures, i.e., abundance of iron species and their ratios, molybdenum (Mo) abundance, and sulfur isotopic data, were used to document the Ediacaran oceanic redox changes in South China (Bristow et al., 2009; McFadden et al., 2008). In contrast, in the absence of metazoan fossils during the Cryogenian Period (750–635 Ma), less attention was paid to the oceanic changes of that time. Here, we use multi-proxies, including ratios of highly reactive iron (Fe_{HR}) to total iron (Fe_T) (Fe_{HR}/Fe_T), pyrite iron (Fe_P) to highly reactive iron (Fe_{HR}) (Fe_P/Fe_{HR}), total iron (Fe_T) to Al (Fe_T/Al), and Mo concentrations, to illustrate the oceanic redox conditions, under which sulfur cycling was discussed as well based on the sulfur isotopic data of pyrite ($\delta^{34}S_{py}$) during the Cryogenian Period in South China.

2. Geological settings

The South China Block is generally considered to have been formed through amalgamation between the Yangtze and Cathaysia blocks during the Sibao orogeny at ca. 1.1–0.9 Ga (Li et al., 2002; Li et al., 2009; Ye et al., 2007), which then experienced episodic rifting between ca. 820 Ma and 542 Ma (Li et al., 2003; Wang and Li, 2003; Wang et al., 2009). A southeast-facing (present orientation) passive continental margin on the Yangtze Block was subsequently developed in the course of breakup of the Rodinia Supercontinent (Fig. 1A). Thermal subsidence related to the post-rift extension of South China Block created significant accommodation space in which thick Middle-to-Late Neoproterozoic successions were deposited (Jiang et al., 2003; Wang and Li, 2003).

Neoproterozoic stratigraphic successions in South China comprise well exposed, relatively unaltered glacial and interglacial deposits (Fig. 1B). The Cryogenian Group unconformably overlies the slate rocks of the Banxi Group. Two main Cryogenian diamictite successions,

* Corresponding author.
E-mail address: feng.lian.jun@gmail.com (L.-J. Feng).

1342-937X/$ – see front matter
doi:10.1016/j.gr.2010.02.011

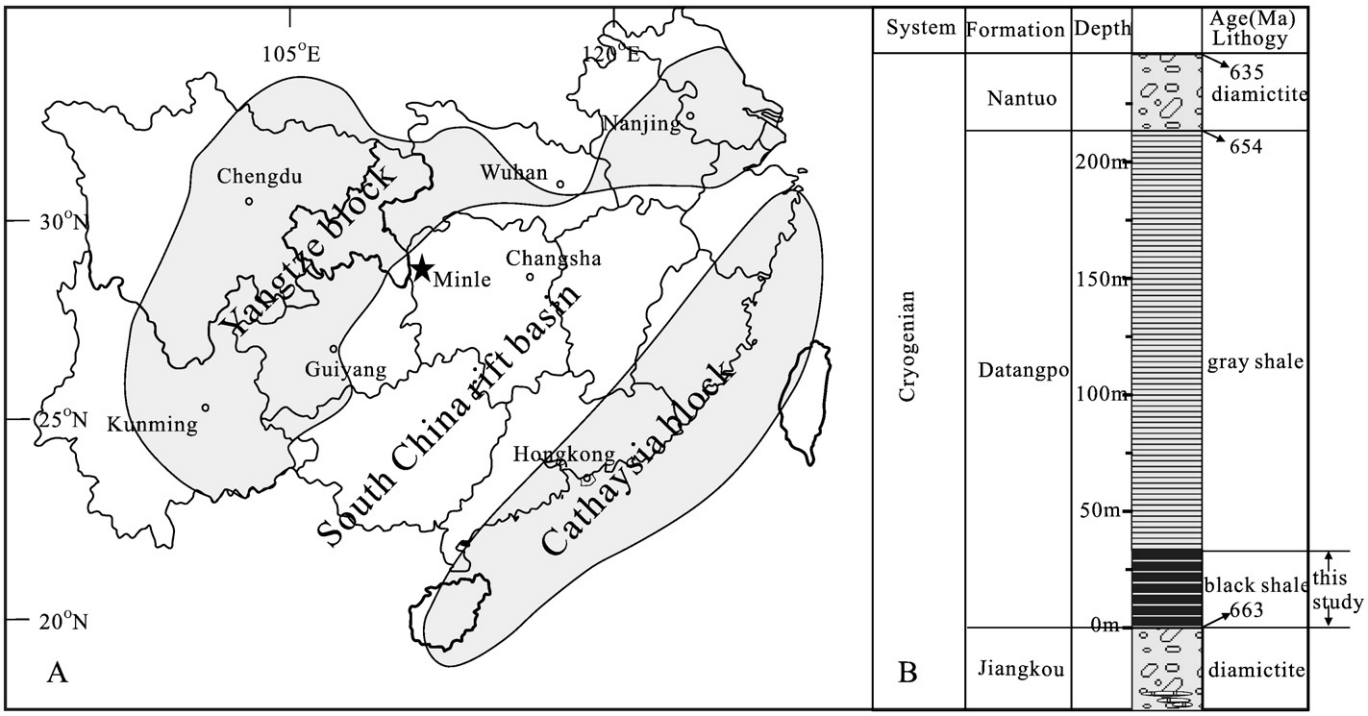

Fig. 1. (A) Cryogenian paleogeography of South China blocks after Jiang et al. (2003); Zhou et al. (2004). (B) Generalized stratigraphic column of the Datangpo Formation in Minle County, Hunan Province, South China. Recent geochronometric ages are discussed in Condon et al. (2005); Zhang et al. (2008); Zhou et al. (2004).

the lower Jiangkou Group and the upper Nantuo Formation, have been recognized in South China. The interglacial Datangpo Formation of manganese-bearing shales, ~10 m thick on the upper slope to ~200 m thick on the lower slope (Wang and Li, 2003), sits on the glacial deposits of the Jiangkou Group. The Datangpo Formation includes the lower thinner black shales (~30 m thick), the focus of this study, and the upper thicker grey shales (~200 m thick) (Fig. 1B). A pair U-Pb zircon ages of 663 ± 4 Ma (Zhou et al., 2004) and 654.5 ± 3.8 Ma (Zhang et al., 2008) for the tuffaceous beds in the basal and topmost Datangpo Formation provides a constraint for the timing of this interglacial interval.

3. Methods

In this study, we choose the Mingle section, where the interglacial Datangpo Formation comprises the lower 30 m-thick black shales and the upper 180 m-thick grey shales (Fig. 1). 16 samples, each at approximately 2 m apart, were collected in the lower 30 m-thick black shales for geochemical analysis. For each sample, ca. 5 g of fresh shale was grinded to powder (200 mesh in size) in an automated agate mill.

Different iron species, including pyrite iron (Fe_P), dithionite-extractable iron (Fe_D) and highly reactive iron (Fe_{HR}), were analyzed in this study. Extraction of Fe_D has followed the method of Canfield (1989). 0.2 g sample powder was firstly digested with a 10 ml buffer solution composed of 58.8 g/l tri-sodium citrate dihydrate ($C_6H_5Na_3O_7 \cdot 2H_2O$) and 20 ml/l acetic acid, then was added with approximate 0.5 g sodium dithionite. The concentrations of dithionite-extractable iron were determined by AAS at Institute of Geology and Geophysics, Chinese Academy of Sciences (IGGCAS). Pyrite iron (Fe_P) was extracted following the chromium reduction method (Canfield et al., 1986; Chu et al., 1994). Approximate 0.5–1.0 g samples were reacted with 40 ml of 1 M $CrCl_2$ in an N_2 gas. H_2S produced from pyrite reduction by $CrCl_2$ was bubbled through a 2% $AgNO_3$ trap where it was precipitated as Ag_2S. The Ag_2S precipitate was dried and weighed to determine the concentration of pyrite sulfur, and the amount of iron bound in pyrite (Fe_P) was calculated with a molar Fe:S ratio of 1:2. Fe_{HR} was determined by calculating through the relation as $Fe_{HR} = Fe_P + Fe_D$.

Major elements, including total iron content (Fe_T), and Al were measured by X-ray fluorescence (XRF). Ca. 1.2 g power samples were weighted and burned in a muffle oven at 1000 °C for the removal of organic carbon and pyrite in the samples. The residues were mixed with 6.0 g of $Li_2B_4O_7$, and fused to glass beads in Pt crucibles at 1100 °C. All the beads were analyzed by XRF-1500 Sequential X-ray Fluorescence Spectrometer (SHIMADZU Inc.) at IGGCAS.

Element Mo was extracted from bulk, dried powders using HF/HNO_3/$HClO_4$ digestions. We analyze it for molybdenum on ICP-MS Element at IGGCAS. A set of Chinese national and USGS rock standard, GBW07107 (shale) and GXR5 (soil), were chosen for calibrating element concentrations of unknowns. Analytical accuracy is better than 5%.

For sulfur isotope analysis, Ag_2S precipitate above was homogenized with cupric oxide and combusted under vacuum for a conversion to sulfur dioxide (approximate 15 mg of Ag_2S and 150 mg of Cu_2O were combusted at 1050 °C for 15 min and analyzed at IGGCAS on a Finnigan Delta S gas source mass spectrometer). Sulfur isotope results are generally reproducible within ±0.3‰.

Total carbon (TC%) and total inorganic carbon (TIC%) concentrations were measured with an Elementar high TOC 2 at IGGCAS. A Chinese national rock standard, GBW07402, was used. Accuracy was better than 3% for TC and TIC concentrations. TOC (total organic carbon) content is calculated by subtracting TIC from TC.

4. Results and discussions

4.1. Paleo-redox conditions

4.1.1. Ratios of iron species

Ratios of different iron species, i.e., Fe_{HR}/Fe_T, Fe_P/Fe_{HR} and Fe_T/Al ratios, are illustrated in Fig. 2 and Table 1. Fe_{HR}/Fe_T ratios in the black shales of studied horizon vary from 0.10 to 0.88, averaging 0.50, in which three short-term negative spikes (N1 to N3) are unraveled, showing fluctuant variations of Fe_{HR}/Fe_T ratios. Fe_P/Fe_{HR} ratios vary

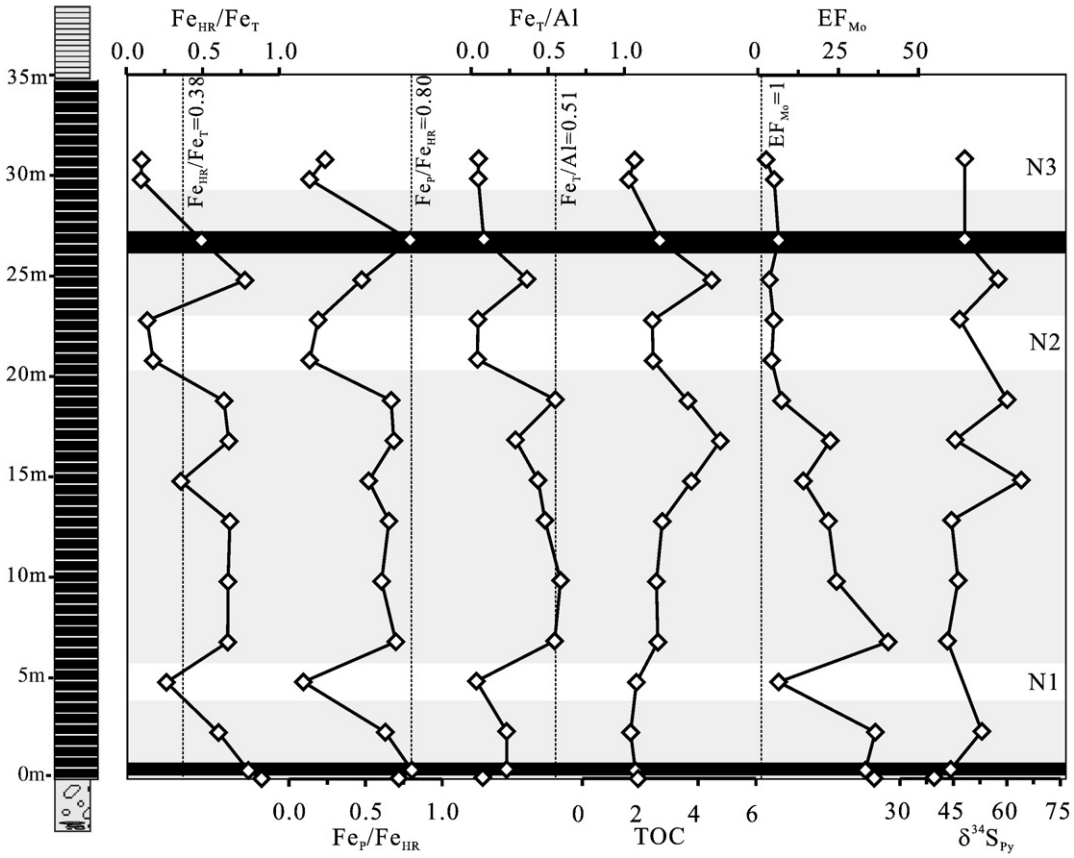

Fig. 2. Geochemical data including Fe_{HR}/Fe_T; Fe_P/Fe_{HR}; Fe_T/Al; and EF_{Mo}; organic matter content (TOC) and pyrite sulfur isotope ($\delta^{34}S_{Py}$) in the Datangpo black shales of the Minle section, Hunan Province. Redox conditions are shown by shaded backgrounds in: euxinia = dark, non-sulfidic anoxia (ferruginous) = light gray, oxic conditions = white.

from 0.09 to 0.80, averaging 0.50, mimicking well the variation pattern of Fe_{HR}/Fe_T ratios. Fe_T/Al ratios vary from 0.03 to 0.58, averaging 0.25, similarly following the variation patterns of those ratios listed above.

Modern sediments deposited under an oxic water column generally produce a low proportion of Fe_{HR} relative to Fe_T contents, yielding a Fe_{HR}/Fe_T ratio of 0.38 (Raiswell and Canfield, 1998; Wijsman et al., 2001a). In contrast, sediments accumulated under an anoxic water column can have a higher proportion of Fe_{HR}, thereby yielding a Fe_{HR}/Fe_T ratio greater than 0.38. Accordingly, most of our Fe_{HR}/Fe_T ratios are greater than 0.38, suggesting an overall anoxic conditions (Fig. 2). However, the appearance of three short-term negative spikes with Fe_{HR}/Fe_T ratios <0.38 indicates multiple incursions of oxic water masses in the context of anoxic water conditions. Furthermore, the upward decrease in Fe_{HR}/Fe_T ratios and increase in the timing for negative spikes (Fig. 2) implicate an overall oxygenating, although episodic, trend in oceanic condition. This scenario is further corroborated by the overlying grey shale successions corresponding to a sea level fall prelude to the Marinoan glaciation.

The Fe_P/Fe_{HR} ratio is a proxy representing the extent to which Fe_{HR} has been converted to pyrite (Anderson and Raiswell, 2004). Evidence from the Black Sea and other euxinic (or sulfidic) basins shows that

Table 1
Geochemical data of the black shales from the Datangpo Formation.

Sample	Lithology	Depth (m)	Fe_P (wt.%)	Fe_D (wt.%)	Fe_T (wt.%)	Fe_{HR}/Fe_T (wt.%/wt.%)	Fe_P/Fe_{HR} (wt.%/wt.%)	TOC (wt.%)	TIC (wt.%)	Fe_T/Al (wt.%/wt.%)	Mo (ppm)	Mo/Al (ppm/wt.%)	EF_{Mo}	Al (wt.%)	$\delta^{34}S_{pyr}$ (‰)
ML56	Black shale	30.8	0.01	0.03	0.39	0.10	0.24	1.81	0.00	0.05	2	0.25	2.5	8.03	48.2
ML57	Black shale	29.8	0.00	0.03	0.36	0.10	0.13	1.61	0.00	0.05	4	0.50	5.0	7.96	–
ML60	Black shale	26.8	0.30	0.08	0.78	0.49	0.79	2.68	0.00	0.08	6	0.64	6.4	9.39	48.2
ML62	Black shale	24.8	1.12	1.24	3.05	0.77	0.48	4.47	0.02	0.36	3	0.36	3.6	8.38	57.6
ML64	Black shale	22.8	0.01	0.04	0.36	0.14	0.19	2.42	0.00	0.04	4	0.50	5.0	8.07	46.8
ML66	Black shale	20.8	0.01	0.06	0.39	0.18	0.13	2.44	0.00	0.04	4	0.43	4.3	9.38	–
ML68	Black shale	18.8	1.91	0.95	4.48	0.64	0.67	3.64	0.04	0.55	6	0.74	7.4	8.14	60.1
ML70	Black shale	16.8	1.07	0.49	2.32	0.67	0.69	4.77	0.01	0.29	18	2.25	22.5	8.01	45.5
ML72	Black shale	14.8	0.68	0.63	3.68	0.36	0.52	3.77	0.01	0.43	12	1.42	14.2	8.47	64.0
ML74	Black shale	12.8	1.94	1.03	4.39	0.68	0.65	2.77	0.05	0.48	20	2.20	22.0	9.10	44.5
ML77	Black shale	9.8	2.11	1.37	5.24	0.66	0.61	2.56	0.05	0.58	22	2.45	24.5	8.97	46.3
ML79	Black shale	6.8	1.92	0.83	4.16	0.66	0.70	2.61	0.05	0.54	31	4.06	40.6	7.63	43.3
ML80	Black shale	4.8	0.01	0.09	0.38	0.26	0.09	1.87	0.04	0.03	7	0.64	6.4	10.95	–
ML81	Black shale	2.3	0.70	0.41	1.83	0.60	0.63	1.67	0.03	0.23	29	3.65	36.5	7.94	53.0
ML82	Black shale	0.4	1.64	0.40	2.56	0.80	0.80	1.84	0.03	0.23	37	3.35	33.5	11.04	44.3
ML83	Black shale	0	0.38	0.15	0.60	0.88	0.72	1.92	0.00	0.08	29	3.62	36.2	8.01	39.6

sediments deposited there commonly yield Fe_P/Fe_{HR} ratios greater than 0.80 (Anderson and Raiswell, 2004); those deposited under anoxic, ferruginous water columns generally have Fe_P/Fe_{HR} ratios less than 0.80 (Canfield et al., 2008; Poulton et al., 2004). Our data show that most of the samples with elevated Fe_{HR}/Fe_T ratios (>0.38) have Fe_P/Fe_{HR} ratios <0.80 (Fig. 2), suggesting an overall anoxic (ferruginous) rather than euxinic water columns under which the black shales were deposited, reconciling the redox condition as stated above. This oceanic condition is supported by evidence elsewhere, i.e., in the synchronous outer shelf and deep basin of Canada, Greenland, where Fe_{HR}/Fe_T ratios are greater than 0.38, but Fe_P/Fe_{HR} ratios are less than 0.80 (Canfield et al., 2008). However, we note that Fe_P/Fe_{HR} ratios for two samples (ML82, and ML60) approximating 0.8 could suggest the episodic occurrence of water column intermittent euxinia during the deposition of the black shales, reflecting a local or basin-scale scenario.

In addition, Fe_T/Al is also useful as a paleo-redox proxy (Lyons and Severmann, 2006). The typical modern euxinic basin like the Black Sea has the elevated Fe_T/Al ratios (0.6 to 1.2) (Lyons and Severmann, 2006). Throughout the Datangpo black shales, Fe_T/Al ratios are generally less than or approximate those of the average shales ($Fe_T/Al = 0.51$) (Fig. 2) (Taylor and McLennan, 1985). Therefore, together with the ratios of different iron species of the Datangpo black shales as mentioned above, Fe_T/Al ratios further confirm that water column may not be persistent euxinia during the deposition of the Datangpo black shales.

4.1.2. Mo concentrations

In the ocean, Mo exists primarily as the soluble molybdate complex (MoO_4^{2-}). A critical activity of hydrogen sulfide (ca. 50–250 uM HS^-) would facilitate conversion of molybdate (MoO_4^{2-}) to thiomolybdates ($MoO_{4-x}S_x^{2-}$) that are subsequently scavenged by sedimentary particles (Helz et al., 1996; Zheng et al., 2000). Because of the low background values (ca. 1–2 ppm), Mo is the most sensitive redox elements compared to the other trace metals. In order to discern the redox conditions, the elemental compositions are usually compared after normalizing the trace metal concentrations to Al, a proxy for aluminosilicate detritus (Tribovillard et al., 2006; Van der Weijden, 2002). In addition, trace metal (TM) concentrations are expressed in terms of enrichment factors (EF_{TM}), where the Al-normalized metal concentration is compared to the average shale values (Wedepohl, 1971, 1991): $EF_{TM} = TM/Al_{sample}:TM/Al_{average\ shale}$. When $EF_{TM} > 1$, the trace metal of interest is enriched relative to average shale.

Fig. 2 and Table 1 illustrate that enrichment in molybdenum occurs throughout the Datangpo black shales ($2.5 < EF_{Mo} < 40.6$, average = 16.9). Additionally, the molybdenum concentrations show a decreasing trend, reconciling the oxic conditions suggested by different iron species ratios. On the other hand, we note that molybdenum concentrations and iron species ratios do not show similar fluctuations throughout the black shales. Therefore, molybdenum enrichment throughout the black shales may not be simply governed by the benthic redox potential in the late anoxic intervals. In fact, authigenic molybdenum enrichment requires the accumulation of free H_2S as well as a source of dissolved Mo (MoO_4^{2-}) (Tribovillard et al., 2006). For example, during the Archean Eon, the low molybdenum concentrations (2–5 ppm) in the persistent euxinic water column could owe to small amounts of dissolved Mo (MoO_4^{2-}) resulting from weak oxidative weathering of continental materials (Scott et al., 2008). In the case, little molybdenum enrichment in the late anoxic intervals possibly results from decrease dissolved Mo (MoO_4^{2-}) owing to massive uptake by anoxic sediments.

4.2. Pyrite sulfur isotope and sulfur cycling

Fig. 2 illustrates that the Datangpo black shales are characterized by super heavy $\delta^{34}S_{Py}$ values, ranging from 39.6 to 64.0‰ (average: 44.0‰). Coeval sediment pyrites from the Xiangmeng, Zhailanggou and Tanganshan sections in South China rift basin are also enriched in ^{34}S as those of the Minle section (Fig. 3) (Chen et al., 2008; Liu et al., 2006).

In the marine environment, metastable iron sulfides and ultimately pyrite are formed and stored in the sediments (Berner, 1970; Berner, 1984) when H_2S released by bacterial sulfate reduction (BSR) encounters reactive iron. During bacterial sulfate reduction (BSR), ^{32}S is preferentially reduced from source sulfate, producing a ^{32}S-riched sulfide (H_2S) product (Canfield, 2001; Kaplan and Rittenberg, 1964). The reaction of iron with H_2S produces little to no isotopic fractionation (Fry et al., 1988; Price and Shieh, 1979). In general, the magnitude of the fractionation between sulfate and sulfide is controlled by sulfate availability. Larger fractionations are typically expressed under non-limiting sulfate concentrations where microbes have a large reservoir of sulfate that allows them to dissimilate ^{32}S preferentially. In cases of the modern ocean like Black Sea with a sulfate concentration of about 28 mM, sulfur isotopic compositions in the shelf and basinal sediments are enriched in light isotope ^{32}S (Wijsman et al., 2001b) (Fig. 3). On the other hand, smaller fractionations and positive $\delta^{34}S_{Py}$ values always occur (i.e. $\delta^{34}S_{Py}$ are equal or close to coeval $\delta^{34}S_{sulfate}$) when sulfate is limiting, i.e., throughout Precambrian time. For example, pyrites from the deep sulfidic basin were enriched in ^{34}S in the Australian Mesoproterozoic Roper Basin (Fig. 3). Therefore, the more ^{34}S-enriched pyrites in the Datangpo black shales likely reflect a lower sulfate concentration in South China rift basin compared to those in the Australian Mesoproterozoic Roper Basin.

Multiple evidence indicate that the sulfate concentrations gradually increase over the Earth history (Anbar and Knoll, 2002; Kah et al., 2004). However, the low sulfate concentrations could exist in the Cryogenian ocean, indicating that the sulfur cycling must significantly change during the Cryogenian Period. During the most severe ice ages in Earth history (Sturtian and Marinoan glaciations), the riverine flux of sulfate to the ocean could decrease because the hydrologic cycle was diminished during the glaciations (Hoffman et al., 1998). When

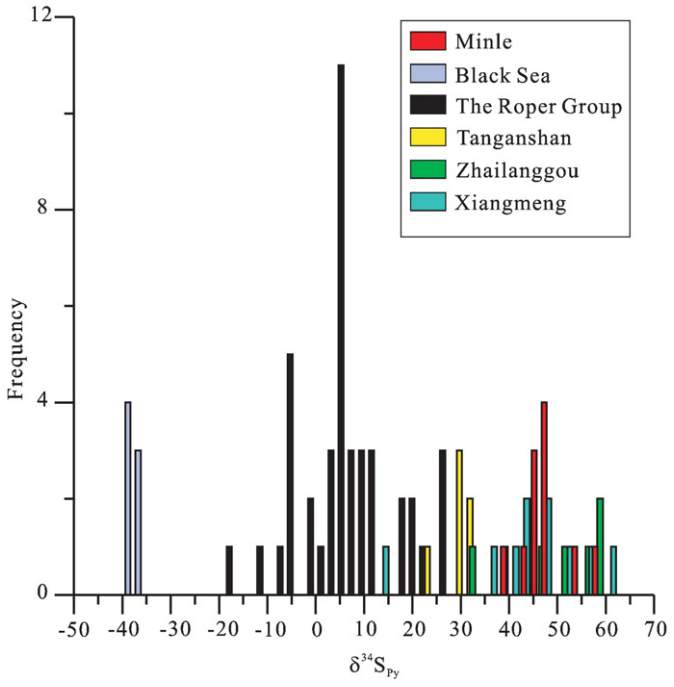

Fig. 3. Pyrite sulfur isotope ($\delta^{34}S_{Py}$) data of the Datangpo black shales (Minle, Zhailanggou, Tanganshan, and Xiangmeng section), the Black Sea and the Roper Group in Australian (Chen et al., 2008; Liu et al., 2006; Shen et al., 2003; Wijsman et al., 2001b).

ocean anoxia developed as a result of extensive ice cover, a substantial portion of the marine sulfate reservoir would have been removed via bacterial sulfate reduction and iron sulfide burial. Generally, as the Sturtian glaciation ended and the hydrologic cycle was reinvigorated, marine sulfate levels should have increased through the interglacial interval due to the enhanced oxidative weathering of continent. Nevertheless, the sulfate reservoir after the glaciation could be still small due to an extremely low background of sulfate concentrations in association with the Sturtian glaciation. Subsequently, the intermittent euxinic conditions stimulated by increase organic flux and sulfate concentrations occurred in the water column during the interglacial interval, suggested by iron species ratios ($Fe_{HR}/Fe_T > 0.38$ and $Fe_P/Fe_{HR} \approx 0.80$). Meanwhile, the marked enrichments of Mo were seen in the lower-20 m Datangpo shales. Similarly, the above scenario appeared in the Archean Eon when low sulfate concentrations and enrichment of molybdenum (maximum value: 40 ppm) also concurrently occurred under a low atmospheric oxygen level (PO_2 is $<10^{-5}$ PAL (present atmospheric level)) (Anbar et al., 2007; Farquhar and Wing, 2003; Pavlov and Kasting, 2004; Reinhard et al., 2009).

5. Conclusions

Multiple ratios between iron species (Fe_{HR}/Fe_T, Fe_P/Fe_{HR}, and Fe_T/Al) and Mo concentrations from the Datangpo black shales suggest that an overall anoxic (ferruginous) condition predominated over the deposition, although several short-term oxic and euxinic episodes interrupted. The superheavy $\delta^{34}S_{Py}$ values suggest a small size of sulfate reservoir during the interglacial epoch. The small-size sulfate reservoir and concurrent enrichment of molybdenum indicate that the ocean chemistry in the Cryogenian Period is similar to that in the Archean Eon.

Acknowledgements

This study is supported by the National Natural Science Foundation of China (grant nos. 40532012, 40603021 and 40373011) and the Chinese Academy of Sciences (grant no. KZCX3-SW-141). The authors would like to thank Daizhao Chen for his critical advice and English improvement on the manuscript. We thank Ganqing Jiang and an anonymous reviewer for thoughtful and constructive comments.

References

Anbar, A.D., Duan, Y., Lyons, T.W., Arnold, G.L., Kendall, B., Creaser, R.A., Kaufman, A.J., Gordon, G.W., Scott, C., Garvin, J., Buick, R., 2007. A whiff of oxygen before the great oxidation event? Science 317, 1903–1906.

Anbar, A.D., Knoll, A.H., 2002. Proterozoic ocean chemistry and evolution: a bioinorganic bridge? Science 297, 1137–1142.

Anderson, T.F., Raiswell, R., 2004. Sources and mechanisms for the enrichment of highly reactive iron in euxinic Black Sea sediments. Am. J. Sci. 304, 203–233.

Berner, R.A., 1970. Pleistocene sea levels possibly indicated by buried black sediments in the Black Sea. Nature 227, 700.

Berner, R.A., 1984. Sedimentary pyrite formation: an update. Geochim. Cosmochim. Acta 48, 605–615.

Bristow, T.F., Kennedy, M.J., Derkowski, A., Droser, M.L., Jiang, G., Creaser, R.A., 2009. Mineralogical constraints on the paleoenvironments of the Ediacaran Doushantuo Formation. Proc. Natl. Acad. Sci. U.S.A. 106, 13190–13195.

Canfield, D.E., 1989. Reactive iron in marine sediments. Geochim. Cosmochim. Acta 53, 619–632.

Canfield, D.E., 2001. Isotope fractionation by natural populations of sulfate-reducing bacteria. Geochim. Cosmochim. Acta 65, 1117–1124.

Canfield, D.E., Poulton, S.W., Knoll, A.H., Narbonne, G.M., Ross, G., Goldberg, T., Strauss, H., 2008. Ferruginous conditions dominated later Neoproterozoic deep-water chemistry. Science 321, 949–952.

Canfield, D.E., Poulton, S.W., Narbonne, G.M., 2007. Late-Neoproterozoic deep-ocean oxygenation and the rise of animal life. Science 315, 92–95.

Canfield, D.E., Raiswell, R., Westrich, J.T., Reaves, C.M., Berner, R.A., 1986. The use of chromium reduction in the analysis of reduced inorganic sulfur in sediments and shales. Chem. Geol. 54, 149–155.

Chen, J.Y., Oliveri, P., Li, C.W., Zhou, G.Q., Gao, F., Hagadorn, J.W., Peterson, K.J., Davidson, E.H., 2000. Precambrian animal diversity: putative phosphatized embryos from the Doushantuo formation of China. Proc. Natl. Acad. Sci. U.S.A. 97, 4457–4462.

Chen, X., Li, D., Ling, H.F., Jiang, S.Y., 2008. Carbon and sulfur isotopic compositions of basal Datangpo Formation, northeastern Guizhou, South China: implications for depositional environment. Prog. Nat. Sci. 18, 421–429.

Chu, X.L., Zhao, R., Zang, W.X., Lei, J.J., Tang, Y.G., 1994. Extraction of various sulfurs in coal and sedimentary rock and preparation of samples for sulfur isotopic analysis. Chinese. Sci. Bull. 39, 140–145.

Condon, D., Zhu, M.Y., Bowring, S., Wang, W., Yang, A.H., Jin, Y.G., 2005. U-Pb ages from the neoproterozoic Doushantuo Formation, China. Science 308, 95–98.

Farquhar, J., Wing, B.A., 2003. Multiple sulfur isotopes and the evolution of the atmosphere. Earth Planet. Sci. Lett. 213, 1–13.

Fike, D.A., Grotzinger, J.P., Pratt, L.M., Summons, R.E., 2006. Oxidation of the Ediacaran Ocean. Nature 444, 744–747.

Fry, B., Gest, H., Hayes, J.M., 1988. $^{34}S/^{32}S$ fractionation in sulfur cycles catalyzed by anaerobic bacteria. Appl. Environ. Microbiol. 54, 250–256.

Helz, G.R., Miller, C.V., Charnock, J.M., Mosselmans, J.F.W., Pattrick, R.A.D., Garner, C.D., Vaughan, D.J., 1996. Mechanism of molybdenum removal from the sea and its concentration in black shales: EXAFS evidence. Geochim. Cosmochim. Acta 60, 3631–3642.

Hoffman, P.F., Kaufman, A.J., Halverson, G.P., Schrag, D.P., 1998. A Neoproterozoic snowball earth. Science 281, 1342–1346.

Jiang, G.Q., Sohl, L.E., Christie-Blick, N., 2003. Neoproterozoic stratigraphic comparison of the Lesser Himalaya (India) and Yangtze block (south China): Paleogeographic implications. Geology 31, 917–920.

Kah, L.C., Lyons, T.W., Frank, T.D., 2004. Low marine sulphate and protracted oxygenation of the Proterozoic biosphere. Nature 431, 834–838.

Kaplan, I.R., Rittenberg, S.C., 1964. Microbiological fractionation of sulfur isotopes. J. Gen. Microbiol. 34, 195–212.

Komiya, T., Hirata, T., Kitajima, K., Yamamoto, S., Shibuya, T., Sawaki, Y., Ishikawa, T., Shu, D., Li, Y., Han, J., 2008. Evolution of the composition of seawater through geologic time, and its influence on the evolution of life. Gondwana Res. 14, 159–174.

Li, Y., Guo, J., Zhang, X., Zhang, W., Liu, Y., Yang, W., Li, Y., Liu, L., Shu, D., 2008. Vase-shaped microfossils from the Ediacaran Weng'an biota, Guizhou, South China. Gondwana Res. 14, 263–268.

Li, X.H., Li, W.X., Li, Z.X., Lo, C.H., Wang, J., Ye, M.F., Yang, Y.H., 2009. Amalgamation between the Yangtze and Cathaysia Blocks in South China: constraints from SHRIMP U-Pb zircon ages, geochemistry and Nd-Hf isotopes of the Shuangxiwu volcanic rocks. Precambrian Res. 174, 117–128.

Li, Z.X., Li, X.H., Kinny, P.D., Wang, J., Zhang, S., Zhou, H., 2003. Geochronology of Neoproterozoic syn-rift magmatism in the Yangtze Craton, South China and correlations with other continents: evidence for a mantle superplume that broke up Rodinia. Precambrian Res. 122, 85–109.

Li, Z.X., Li, X.H., Zhou, H.W., Kinny, P.D., 2002. Grenvillian continental collision in south China: new SHRIMP U-Pb zircon results and implications for the configuration of Rodinia. Geology 30, 163–166.

Liu, T.B., Maynard, J.B., Alten, J., 2006. Superheavy S Isotopes from Glacier-Associated Sediments of the Neoproterozoic of South China: Oceanic Anoxia or Sulfate Limitation? In: Kesler, S.E., Ohmoto, H. (Eds.), Evolution of Early Earth's Atmosphere, Hydrosphere, and Biosphere-Constraints from Ore Deposits: Geological Society of America Memoir, pp. 205–222.

Lyons, T.W., Severmann, S., 2006. A critical look at iron paleoredox proxies: new insights from modern euxinic marine basins. Geochim. Cosmochim. Acta 70, 5698–5722.

Maruyama, S., Santosh, M., 2008. Models on snowball earth and cambrian explosion: a synopsis. Gondwana Res. 14, 22–32.

McFadden, K.A., Huang, J., Chu, X., Jiang, G., Kaufman, A.J., Zhou, C., Yuan, X., Xiao, S., 2008. Pulsed oxidation and biological evolution in the Ediacaran Doushantuo Formation. Proc. Natl. Acad. Sci. U.S.A. 105, 3197–3202.

Ohno, T., Komiya, T., Ueno, Y., Hirata, T., Maruyama, S., 2008. Determination of $^{88}Sr/^{86}Sr$ mass-dependent isotopic fractionation and radiogenic isotope variation of $^{87}Sr/^{86}Sr$ in the Neoproterozoic Doushantuo Formation. Gondwana Res. 14, 126–133.

Pavlov, A.A., Kasting, J.F., 2004. Mass-independent fractionation of sulfur isotopes in Archean sediments: strong evidence for an anoxic Archean atmosphere. Astrobiology 2, 27–41.

Poulton, S.W., Fralick, P.W., Canfield, D.E., 2004. The transition to a sulphidic ocean approximately 1.84 billion years ago. Nature 431, 173–177.

Price, F.T., Shieh, Y.N., 1979. Fractionation of sulfur isotopes during laboratory synthesis of pyrite at low temperatures. Chem. Geol. 27, 245–253.

Raiswell, R., Canfield, D.E., 1998. Sources of iron for pyrite formation in marine sediments. Am. J. Sci. 298, 219–245.

Reinhard, C.T., Raiswell, R., Scott, C., Anbar, A.D., Lyons, T.W., 2009. A late Archean Sulfidic Sea stimulated by early oxidative weathering of the continents. Science 326, 713–716.

Scott, C., Lyons, T.W., Bekker, A., Shen, Y., Poulton, S.W., Chu, X., Anbar, A.D., 2008. Tracing the stepwise oxygenation of the Proterozoic ocean. Nature 452, 456–459.

Shen, Y., Knoll, A.H., Walter, M.R., 2003. Evidence for low sulphate and anoxia in a mid-Proterozoic marine basin. Nature 423, 632–635.

Taylor, S.R., McLennan, S.M., 1985. The Continental Crust: Its Composition and Evolution. Blackwell Scientific Pub, Palo Alto, CA, United States.

Tribovillard, N., Algeo, T.J., Lyons, T., Riboulleau, A., 2006. Trace metals as paleoredox and paleoproductivity proxies: an update. Chem. Geol. 232, 12–32.

Van der Weijden, C.H., 2002. Pitfalls of normalization of marine geochemical data using a common divisor. Mar. Geol. 184, 167–187.

Wang, J., Li, Z.X., 2003. History of Neoproterozoic rift basins in South China: implications for Rodinia break-up. Precambrian Res. 122, 141–158.

Wang, X.C., Li, X.H., Li, W.X., Li, Z.X., 2009. Variable involvements of mantle plumes in the genesis of mid Neoproterozoic basaltic rocks in South China: a review. Gondwana Res. 15, 381–395.

Wedepohl, K.H., 1971. Environmental Influences on the Chemical Composition of Shales and Clays. In: Ahrens, L.H. (Ed.), Physics and Chemistry of the Earth. Elsevier, Oxford, pp. 305–333.
Wedepohl, K.H., 1991. The Composition of the Upper Earth's Crust and the Natural Cycles of Selected Metals. In: Merian, E. (Ed.), Metals and their Compounds in the Environment. VCH-Verlagsgesellschaft, Weinheim, pp. 3–17.
Wijsman, J.W.M., Middelburg, J.J., Heip, C.H.R., 2001a. Reactive iron in Black Sea Sediments: implications for iron cycling. Mar. Geol. 172, 167–180.
Wijsman, J.W.M., Middelburg, J.J., Herman, P.M.J., Bottcher, M.E., Heip, C.H.R., 2001b. Sulfur and iron speciation in surface sediments along the northwestern margin of the Black Sea. Mar. Chem. 74, 261–278.
Xiao, S.H., Zhang, Y., Knoll, A.H., 1998. Three-dimensional preservation of algae and animal embryos in a Neoproterozoic phosphorite. Nature 391, 553–558.
Ye, M.F., Li, X.H., Li, W.X., Liu, Y., Li, Z.X., 2007. SHRIMP zircon U-Pb geochronological and whole-rock geochemical evidence for an early Neoproterozoic Sibaoan magmatic arc along the southeastern margin of the Yangtze Block. Gondwana Res. 12, 144–156.
Zhang, S., Jiang, G., Han, Y., 2008. The age of the Nantuo Formation and Nantuo glaciation in South China. Terra Nova 20, 289–294.
Zheng, Y., Anderson, R.F., van Geen, A., Kuwabara, J., 2000. Authigenic molybdenum formation in marine sediments: a link to pore water sulfide in the Santa Barbara Basin. Geochim. Cosmochim. Acta 64, 4165–4178.
Zhou, C.M., Tucker, R., Xiao, S.H., Peng, Z.X., Yuan, X.L., Chen, Z., 2004. New constraints on the ages of Neoproterozoic glaciations in South China. Geology 32, 437–440.